Food Chemistry 525 (2026) 150491

Contents lists available at ScienceDirect

Food Chemistry

journal homepage: www.elsevier.com/locate/foodchem

Integrated multi-elemental and $^{87}Sr/^{86}Sr$ isotopic fingerprinting coupled with explainable artificial intelligence for geographical authentication of wheat☆

Giulia Puzo [a,b,*], Tea Zuliani [c], Michele Magarelli [d], Pierfrancesco Novielli [e], Emilia Pucci [b], Valeria Poscente [b], Alessandra Bernardini [b], Sabina Tangaro [d,e], Massimo Reverberi [a], Claudia Zoani [b]

[a] Department of Environmental Biology (DBA), Sapienza University of Rome, Rome, Italy
[b] Department for Sustainability, Sustainable Agri-Food Systems Division (SSPT-AGROS), Italian National Agency for New Technologies, Energy and Sustainable Economic Development (ENEA), Casaccia Research Centre, Rome, Italy
[c] Department of Environmental Sciences, Jožef Stefan Institute, Ljubljana, Slovenia
[d] Department of Soil, Plant and Food Sciences, University of Bari Aldo Moro, Bari, Italy
[e] National Institute for Nuclear Physics, (INFN), Section of Bari, Italy

ARTICLE INFO

Keywords:
Wheat
Geographical authentication
$^{87}Sr/^{86}Sr$ ratio
Multi-element fingerprinting
Random forest
SHAP

ABSTRACT

This study presents an integrated framework combining multi-elemental profiling and $^{87}Sr/^{86}Sr$ isotopic fingerprinting with machine learning and explainable artificial intelligence (XAI) for the geographical authentication of Italian wheat. A total of 122 samples collected from Northern, Central and Southern Italy over two harvest years (2023–2024) were analysed by ICP–MS and MC–ICP–MS. Elemental composition exhibited pronounced interannual variability, whereas the $^{87}Sr/^{86}Sr$ ratio showed greater temporal stability and a consistent link to geological background. Random Forest models achieved three-class classification accuracies of 0.75 ± 0.08 for 2023 data and 0.81 ± 0.06 for 2024. SHAP analysis identified the isotopic ratio, together with Zn, Ni, Mn and Cu, as the main contributors to classification. Results demonstrate that wheat geographical origin is reliably characterised by an integrated elemental–isotopic signature interpreted through explainable machine learning, supporting provenance assessment across the major Italian macro-areas over different harvest years.

1. Introduction

Food traceability and authenticity have become global priorities. The growing internationalisation of food trade and the increasing complexity of supply chains have amplified the risk of fraud and mislabelling, with direct consequences for consumer safety and trust, as well as the competitiveness of local production systems (Hassoun et al., 2023). Cereals are among the most vulnerable commodities, as they are staple foods widely traded across international markets, making reliable tools for verifying their geographical origin essential for consumer protection and for safeguarding producers' interests (Telloli et al., 2024).

Italy plays a central role in the production of durum and common wheat, which are the primary raw materials for pasta and bread. However, the widespread importation of foreign wheat and global competition expose Italian supply chains to potential provenance fraud (FAO, 2023). Establishing the geographical origin of wheat with scientific accuracy is therefore critical, not only to ensure transparency for consumers but also to protect local production systems and to support quality certification schemes such as Protected Designation of Origin (PDO) and Protected Geographical Indication (PGI), which rely on verified origin claims (Magarelli et al., 2024; Tsirogiannis et al., 2023; Zhao et al., 2011). In this context, analytical approaches that provide reliable and reproducible evidence of origin are increasingly demanded by regulatory authorities and certification bodies.

Several analytical strategies have been employed in recent years to establish the elemental and isotopic fingerprinting of foodstuffs. Inductively Coupled Plasma Mass Spectrometry (ICP–MS) has emerged as a reference technique due to its sensitivity and ability to provide

☆ This article is part of a Special issue entitled: '8th IMEKOFOODS' published in Food Chemistry.

* Corresponding author at: Department of Environmental Biology (DBA), Sapienza University of Rome, Piazzale Aldo Moro 5, 00185 Rome, Italy.
E-mail address: giulia.puzo@uniroma1.it (G. Puzo).

https://doi.org/10.1016/j.foodchem.2026.150491
Received 23 March 2026; Received in revised form 8 July 2026; Accepted 18 July 2026
Available online 19 July 2026

comprehensive multi-elemental profiles, and has been successfully applied to cereals and wheat flours to reveal patterns linked to geographical provenance (Nguyen et al., 2023; Thabit et al., 2020; Zhao et al., 2013). Furthermore, the strontium isotope ratio ($^{87}Sr/^{86}Sr$), measured using Multi-Collector ICP–MS, provides a powerful geochemical marker closely linked to the bedrock and soils in which crops are grown. This parameter has been successfully exploited in the authentication of products such as wines, olive oils and cereals (Coelho et al., 2023; Furdek Turk et al., 2022). Because strontium isotopes are transferred from soils to plants with minimal fractionation, the $^{87}Sr/^{86}Sr$ ratio can be considered a particularly robust tracer of geographical origin (Capo et al., 1998; Voerkelius et al., 2010). In contrast, trace-element concentrations in wheat grains are influenced by soil mineralogy, pedological conditions and agronomic factors regulating element availability and transfer to plants (Kabata-Pendias, 2011; White & Broadley, 2009; Zhao et al., 2009). However, datasets simultaneously integrating multi-elemental composition and $^{87}Sr/^{86}Sr$ isotope ratios for wheat across different Italian regions and multiple harvest years remain limited, representing a bottleneck for the development of robust and transferable traceability models.

Most previous studies have relied on traditional chemometric methods, such as Principal Component Analysis (PCA), Linear Discriminant Analysis (LDA), and Partial Least Squares Discriminant Analysis (PLS–DA), to reduce data dimensionality and classify samples (Durante et al., 2013; González-Domínguez et al., 2022; Roberts & Cozzolino, 2016). While these approaches provide useful descriptive power, they assume linear relationships among variables and often fail to capture the complexity of datasets characterised by non-linearity and multicollinearity. Furthermore, the robustness of classification models has seldom been assessed in different harvest years, even though temporal stability is essential for the practical implementation of food traceability tools.

The adoption of machine learning has improved predictive performance in food authenticity research, with algorithms such as Random Forest (RF), Support Vector Machines (SVM) and Gradient Boosting (GB) widely recognised for their effectiveness (González-Domínguez et al., 2022; Granato et al., 2018). However, the limited interpretability of these models remains a major obstacle to their broader use. The recent development of Explainable Artificial Intelligence (XAI) methods, particularly SHAP (SHapley Additive exPlanations), provides a means to quantify the contribution of individual variables and to make model decisions transparent (Bagnulo et al., 2025; Buyuktepe et al., 2023; Lundberg et al., 2020), thereby enabling a direct chemical interpretation of the results. Despite their potential, XAI approaches have so far been only marginally explored in wheat authentication studies and rarely applied to integrated elemental and isotopic datasets, particularly compared with other commodities (Adadi & Berrada, 2018; Buyuktepe et al., 2023; Lundberg et al., 2020; Magarelli et al., 2026). Despite these advances, a clear gap remains in the development of robust and interpretable models for wheat traceability.

This study presents an integrated analytical framework combining ICP–MS and MC–ICP–MS analyses with machine learning to discriminate wheat samples from Northern, Central and Southern Italy. Multi-elemental composition and $^{87}Sr/^{86}Sr$ isotope ratios are jointly modelled within a single predictive approach. Independent datasets from two consecutive harvest years (2023 and 2024) were analysed as separate case studies to evaluate both spatial discrimination and temporal robustness under different environmental conditions, while SHAP-based explainable artificial intelligence was applied to interpret the chemical drivers underlying geographical classification and to clarify the relative contribution of elemental and isotopic variables. In particular, elements such as Zn, Ni, Mn and Cu are known to respond to pedological and environmental controls and may therefore contribute to geographically structured variability in cereal crops (Alves et al., 2016). Although previous studies have demonstrated the usefulness of multi-elemental fingerprinting and strontium isotope ratios for wheat provenance assessment (Bacher et al., 2023; Nguyen et al., 2023; Zhao et al., 2013), most investigations relied on conventional chemometric approaches such as PCA, LDA or PLS–DA (Durante et al., 2013; González-Domínguez et al., 2022; Roberts & Cozzolino, 2016; Marini, 2009), while applications of explainable machine-learning methods to interpret environmental drivers of geographical discrimination in wheat remain limited compared with other food matrices (Buyuktepe et al., 2023; Lundberg et al., 2020; Magarelli et al., 2024). The present study addresses these gaps by integrating multi-elemental composition and $^{87}Sr/^{86}Sr$ isotopic ratios across two harvest years and applying explainable artificial intelligence to link classification performance with pedogeochemical controls on wheat grain composition.

Accordingly, this study tests the hypothesis that geographically structured variability in lithology-dependent Sr isotope signatures and in the bioavailable soil trace-element pool is recorded in wheat grain composition and can support mechanistically interpretable macro-area provenance discrimination. Multi-elemental profiles obtained by ICP–MS and $^{87}Sr/^{86}Sr$ isotope ratios measured by MC–ICP–MS were integrated within a Random Forest classification framework and interpreted using SHAP-based explainable artificial intelligence. This integrated multi-analytical and explainable modelling framework provides a process-informed approach for interpreting geographically structured variability in wheat composition across major Italian geological domains.

2. Materials and methods

2.1. Study area and sampling sites

A total of 122 wheat samples were collected over two consecutive harvest years, 2023 (41 samples) and 2024 (81 samples), ensuring broad geographical coverage and enabling assessment of the temporal robustness of the proposed traceability framework. Overall, the dataset comprised 55 samples from Northern Italy, 35 from Central Italy and 32 from Southern Italy. The 2023 sampling campaign included 12 northern, 13 central and 16 southern samples, whereas the 2024 campaign included 43 northern, 22 central and 16 southern samples. The dataset included both common wheat (*Triticum aestivum* L.) and durum wheat (*Triticum durum* Desf.), comprising 30 and 92 samples, respectively. Their distribution across macro-areas and harvest years was as follows. In 2023, Northern Italy included 9 *T. aestivum* and 3 *T. durum* samples, Central Italy included 8 *T. aestivum* and 5 *T. durum* samples, whereas Southern Italy included only *T. durum* samples ($n = 16$). In 2024, Northern Italy included 8 *T. aestivum* and 35 *T. durum* samples, Central Italy included 5 *T. aestivum* and 17 *T. durum* samples, whereas Southern Italy again included only *T. durum* samples ($n = 16$). Detailed sample metadata, species distribution and cultivar distribution across harvest years and macro-areas are reported in Tables S1–S1c (Supplementary Materials), thereby reflecting the diversity of Italian wheat production systems.

In 2023, wheat samples were collected from the main cereal-growing areas of Italy, covering northern (Piedmont, Lombardy, Veneto, Emilia-Romagna and Friuli Venezia Giulia), central (Tuscany, Marche, Abruzzo and Lazio) and southern regions (Apulia, Basilicata and Sicily). The sampling encompassed both widely cultivated commercial cultivars and locally adapted genotypes, thereby capturing the agronomic and genetic diversity of Italian wheat production systems.

In 2024, the sampling campaign expanded to 81 samples, with a strong focus on durum wheat, reflecting its central role in Italian cereal supply chains and quality-oriented production. Wheat samples were collected from northern (Piedmont, Lombardy, Veneto and Emilia-Romagna), central (Tuscany, Umbria, Abruzzo and Lazio) and southern regions (Apulia and Campania). The sampling encompassed several commercial and experimental durum wheat cultivars, complemented by a smaller number of common wheat samples from northern and central Italy. This targeted sampling strategy aimed to strengthen the

representation of the central and southern regions and enhance the dataset's robustness for evaluating both geographical discrimination and interannual variability. As a result, species composition differed between harvest years and among macro-areas. Nevertheless, the objective of this study was to evaluate geographical discrimination at the macro-area level under realistic supply-chain conditions; accordingly, wheat species and cultivar were not used as primary classification variables.

The 2024 sampling campaign consisted of an independent set of sampling locations aimed at extending geographical coverage and evaluating macro-area discrimination across different cereal-growing environments.

For both sampling years, field collection followed a standardised five-point sampling protocol, in which grain aliquots were collected from the four corners and the centre of each plot and then pooled to obtain a representative composite sample (approximately 1–2 kg). All samples were processed and analysed individually, without pooling across sites or years, to preserve site-specific and interannual variability and to ensure the integrity of the geographical signal. The inclusion of multiple wheat species and cultivars increases dataset heterogeneity and reflects realistic supply-chain conditions, thereby supporting the robustness of the proposed framework. Although the classification framework was developed at the macro-area scale (Northern, Central and Southern Italy), the sampling strategy incorporated multiple cereal-growing regions and diverse wheat species and cultivars within each macro-area, thereby capturing the main pedogeochemical variability of Italian wheat production systems under realistic supply-chain conditions.

2.2. Reagents and materials

For sample preparation and reagent dilution, ultrapure water (18.2 MΩ·cm) from a Direct–Q 5 purification system (Millipore, Watertown, MA, USA) was used throughout the study. Nitric acid (67–69% *w*/w HNO_3, Suprapur) was purchased from Carlo Erba Reagents Srl (Milan, Italy), while hydrogen peroxide (30% w/w H_2O_2, Suprapur) and hydrofluoric acid (40% w/w HF, Suprapur) were purchased from Merck (Darmstadt, Germany).

Multi-element external calibration was performed using a Multi VI standard solution (ICP Standard Certipur, Merck, Darmstadt, Germany). Instrumental accuracy and analytical performance for elemental determinations were verified by analysing the certified reference material SPS–SW1 (trace elements in surface water; Spectrapure Standards, Oslo, Norway). For strontium isotope ratio measurements, NIST SRM 987 (strontium carbonate, National Institute of Standards and Technology, Gaithersburg, MD, USA) reference material was used for calibration and mass bias correction. All laboratory consumables, including digestion vessels, chromatographic columns and sample containers, were made of perfluoroalkoxy (PFA), polypropylene or polytetrafluoroethylene (PTFE). Before use, all materials were cleaned in accordance with established trace-element protocols, including prolonged soaking in diluted nitric acid and thorough rinsing with ultrapure water, to minimise contamination.

2.3. Sample collection and preparation

Wheat samples were collected at the sampling sites and transported to the laboratory under dry conditions. For each sample, approximately 150 g of kernels were processed. Grains were ground to a fine, homogeneous flour using a Retsch ZM 200 Ultra Centrifugal Mill (Haan, Germany) with a 12–tooth stainless steel rotor, operating at 12,000 rpm. The mill was thoroughly cleaned with ethanol and compressed air between samples to minimise cross-contamination. No additional drying was applied prior to milling, as samples were stored under dry conditions and showed no evidence of moisture uptake. Potential contributions from milling and sample preparation were monitored by analysing procedural blanks and certified reference materials (Section 2.4).

The obtained flour was homogenised, transferred into polypropylene containers, and subdivided into aliquots for elemental analysis by ICP–MS and strontium isotopic analysis by MC–ICP–MS. Aliquoting was performed immediately after milling to minimise potential segregation effects and to ensure sample representativeness.

For elemental analysis by ICP–MS, 0.3000 g of wheat flour was accurately weighed into PFA Teflon digestion vessels and subjected to closed-vessel microwave digestion (MARS 6, CEM Corporation, Matthews, NC, USA). Samples were digested with a mixture of 4 mL of suprapure HNO_3 (67–69%), 2 mL of suprapure H_2O_2 (30%), and 0.1 mL of suprapure HF (40%). A small amount of HF was added to ensure complete digestion of silicate-bound elements. The microwave programme consisted of a 20 min ramp to 140 °C (5 min hold), followed by a 20 min ramp to 180 °C (25 min hold), and a final cooling period of 30 min.

After digestion, clear solutions were quantitatively transferred into graduated polypropylene tubes and diluted to 20 mL with Milli–Q water. Procedural blanks were prepared using the same digestion protocol and acid mixture. All samples were prepared in replicates to ensure analytical reproducibility, and replicate digestions were used to assess within-sample variability and overall method precision. Method repeatability was assessed through triplicate digestions followed by ICP–MS analysis. Concentration RSD values ranged between 0.5 and 5%, with median RSD values of approximately 2.1%. QC replicate analyses yielded median RSD values of approximately 3.4%, confirming good analytical precision of the elemental measurements (Table S2, Supplementary Materials).

2.4. Multi-elemental and $^{87}Sr/^{86}Sr$ isotope ratio measurements

Multi-elemental concentrations of selected elements (Al, As, Ba, Ca, Cd, Ce, Co, Cr, Cu, Fe, Hg, La, Mn, Mo, Ni, Pb, Rb, Sn, Sr, Ti, V, Zn and Zr) in wheat samples were determined by inductively coupled plasma mass spectrometry (ICP–MS, 7700× series, Agilent Technologies, Tokyo, Japan), following established multi-elemental and Sr isotopic fingerprinting approaches widely applied in provenance studies (Nikezić, Chantzi, et al., 2024; Nikezić, Perşoiu, et al., 2024). Instrument operating conditions were optimized daily to ensure high sensitivity and signal stability. Measurements were performed using a Micromist nebuliser coupled to a Scott double-pass spray chamber, and helium collision cell mode was used to minimise polyatomic interferences. Rhodium (^{103}Rh) was used as an internal standard to correct for instrumental drift and matrix effects, as it is not naturally present in wheat matrices and provides a stable signal under the applied analytical conditions.

Element quantification was performed using external calibration with certified multi-element standard solutions, and linearity was confirmed by correlation coefficients (R^2) consistently above 0.999. Analytical accuracy for elemental determinations was verified using the matrix-matched certified reference material NIST SRM 1567a (Wheat Flour). In addition, the surface water reference material SPS–SW1 was analysed as an independent quality-control solution to verify instrumental performance.

Procedural blanks were analysed at regular intervals, and limits of detection (LOD) and quantification (LOQ) were calculated as three and ten times the standard deviation of the blanks, respectively. Element-specific LOD and LOQ values ranged from approximately 0.001 to 0.05 ng mL^{-1} and from 0.003 to 0.15 ng mL^{-1}, respectively. Additional analytical performance parameters for ICP–MS measurements are summarised in Supplementary Table S2.

Detailed instrumental operating conditions are provided in Table S3 (Supplementary Materials).

For isotopic analysis, strontium (Sr) was purified from the digested samples prior to measurement. Sample aliquots were evaporated to dryness on a sand bath at temperatures below 90 °C, then the residue was dissolved in 1 mL of 8 mol L^{-1} HNO_3, with 30 min of ultrasonication, and the mixture was subsequently subjected to extraction

chromatography using columns packed with 0.15 g of Sr-selective resin (Eichrom®, 100–150 μm particle size; SR-B200-A, TrisKem International, Brittany, France) to isolate Sr from the sample matrix.

The quality of the chemical separation was assessed by ICP–MS through the determination of residual Rb and recovered Sr in the collected fractions. Rb concentrations in the purified Sr fractions were consistently below 0.01 ng mL^{-1}, whereas Sr levels ranged from 15 to 25 ng mL^{-1}, indicating quantitative recoveries exceeding 95%. Post-column Sr measurements showed ^{88}Sr concentration RSD values ranging between 0.5 and 2%, with median repeatability values of approximately 1.5% (Supplementary Materials, Table S2).

Sr isotope ratios ($^{87}Sr/^{86}Sr$) were measured using a multi-collector inductively coupled plasma mass spectrometer (Nu Plasma II MC–ICP–MS, Ametek, Wrexham, United Kingdom) equipped with an Aridus II desolvating nebuliser system (Teledyne Cetac, Omaha, NE, USA). Instrumental mass fractionation was corrected by internal normalisation to a constant $^{86}Sr/^{88}Sr$ ratio of 0.1194. Contributions from isobaric interferences involving Rb and krypton (Kr) isotopes were corrected mathematically using fixed $^{87}Rb/^{85}Rb$ and $^{86}Kr/^{83}Kr$ ratios of 0.38567 and 1.50566, respectively.

Sr isotope ratio determinations were performed using a standard–sample–standard bracketing protocol with the NIST SRM 987 strontium carbonate reference material at concentrations matched to those of the samples. During the analytical sessions, NIST SRM 987 yielded a mean $^{87}Sr/^{86}Sr$ ratio of 0.709046 ± 0.000054 (2SD), confirming the analytical stability and external precision of the MC–ICP–MS measurements. Triplicate isotopic measurements yielded an isotopic repeatability of approximately ±0.000024 (1SD). Additional analytical performance parameters for MC–ICP–MS measurements are summarised in Supplementary Table S2.

Instrumental operating conditions of the MC–ICP–MS are reported in Table S4 (Supplementary Materials).

2.5. Statistical analysis

2.5.1. Univariate and exploratory multivariate analysis

Data from elemental (ICP–MS) and isotopic (MC–ICP–MS) analyses were analysed separately for each harvest year. Univariate statistical analyses were performed using XLSTAT (Addinsoft, Paris, France).

Principal Component Analysis (PCA) was applied as an unsupervised exploratory technique to the elemental dataset. PCA was performed separately for each harvest year on z-score-standardised elemental concentrations (mean-centred and scaled to unit variance) using XLSTAT, based on the correlation matrix, to explore the multivariate structure of the data and to visualise potential geographical and inter-annual patterns.

For graphical purposes, the same z-score standardisation was applied before boxplot construction to minimise scale effects and allow direct comparison among elements and between harvest years.

Data normality and homogeneity of variances were assessed using the Shapiro–Wilk test and Levene's test, respectively. As most elemental concentrations did not meet the assumptions of normality and homoscedasticity, non-parametric statistical methods were used. Differences among macro-areas were evaluated using the Kruskal–Wallis test.

Statistical significance was set at $p \leq 0.05$, with $p \leq 0.001$ indicating highly significant differences. When the Kruskal–Wallis test indicated significant differences, post hoc pairwise comparisons were performed using Dunn's test with Bonferroni correction for multiple comparisons. Statistically homogeneous groups identified by post hoc analysis are indicated by different letters in the graphical representations, where applicable.

To assess the temporal robustness of the $^{87}Sr/^{86}Sr$ isotopic signature, interannual differences between the 2023 and 2024 datasets were tested within each macro-area using the non-parametric Mann–Whitney *U* test. Exact *p*-values were reported, and multiple testing was corrected for using the Holm correction. This analysis allowed evaluation of year-to-year variability in strontium isotopic composition at both regional and national scales.

Univariate statistical analyses were used to provide an initial descriptive and inferential assessment of spatial and temporal trends and to complement the subsequent multivariate and machine-learning approaches described below. Wheat species and cultivar were not treated as primary classification variables, as the study's objective was to evaluate geographical discrimination under realistic supply-chain conditions, where samples may derive from heterogeneous genetic backgrounds. To assess potential species-related confounding, intra-area comparisons between *Triticum aestivum* and *Triticum durum* were performed separately for each harvest year using the Mann–Whitney *U* test on the main discriminant variables identified by SHAP analysis (Zn, Ni, Mn, Cu and $^{87}Sr/^{86}Sr$).

2.5.2. Chemometrics, machine learning and explainable artificial intelligence

For each experimental year, the final dataset for machine learning modelling was generated by integrating chemical information from ICP–MS analyses with the $^{87}Sr/^{86}Sr$ isotope ratios measured by MC–ICP–MS. The two data sources were merged at the sample level to produce a unified feature matrix for subsequent computational analyses. All data processing, machine learning modelling and explainable artificial intelligence (XAI) analyses were implemented in Python (v. 3.11.10) using fully reproducible scripts to manage dataset integration (ICP–MS and MC–ICP–MS data), feature selection, model training and performance evaluation (Pedregosa et al., 2011). Prior to model development, multicollinearity among predictors was assessed using the Variance Inflation Factor (VIF) with a threshold of 10. An iterative feature selection procedure was applied by progressively removing variables with high VIF values, thereby reducing redundancy and instability in model estimation. This VIF-based filtering was performed prior to model training and consistently applied across the different experimental settings, thereby excluding highly collinear elemental variables. Supervised multi-class classification models based on a Random Forest ensemble algorithm (Breiman, 2001) were developed to predict the macro-area of the samples. These tasks were formulated as independent multi-class classification problems. Input variables were used in their original scale, as tree-based algorithms do not require feature standardisation. Model performance was evaluated using a repeated k-fold cross-validation strategy (Schaffer, 1993). Specifically, a 10 k-fold cross-validation procedure was repeated 20 times with different random partitions of the dataset to ensure robustness and reduce variability associated with data splitting. The model hyperparameters were optimized by exploring a predefined grid, including learning rate values of 0.1, 0.2, 0.3, 0.4, and 0.5; number of estimators ranging from 50 to 500 in steps of 50; and maximum tree depth values of 3, 5, 7, 9, and unlimited depth (None). Classification performance was assessed by calculating the mean values of accuracy (ACC), F1-score (F1), sensitivity (SENS) and specificity (SPEC) across all cross-validation repetitions. Confusion matrices were additionally computed at the sample level to further characterise classification behaviour. The same evaluation framework was consistently applied to all analyses to ensure comparability of results across classification tasks. To support transparency and improve the interpretability of the machine learning models, an explainable artificial intelligence (XAI) approach based on SHapley Additive exPlanations (SHAP) was integrated into the workflow (Lundberg et al., 2020). The reported feature importance values correspond to the mean SHAP values computed across the repeated cross-validation procedure rather than to a single fitted model. Consequently, the reported feature rankings reflect the average contribution of each feature across multiple training/testing splits, reducing the influence of any individual data partition. SHAP analysis was performed on the reduced predictor set obtained after VIF filtering, ensuring that feature attributions were not biased by strongly correlated variables. This approach also improves the stability, consistency, and

interpretability of SHAP explanations. When features are highly correlated, SHAP tends to distribute the attribution of importance across redundant variables, potentially leading to unstable or ambiguous feature contributions (Ning et al., 2022). Given the multi-class setting, SHAP values were evaluated using a one-vs-rest strategy, in which feature contributions were interpreted separately for each target class relative to the remaining two classes. This approach allowed the identification of class-specific elemental and isotopic markers that drive discrimination within each macro-area. The XAI analysis aimed to identify the most informative elemental and isotopic variables contributing to the classification decision process, thereby enabling a chemically meaningful interpretation of the model outputs and supporting the identification of relevant geographical and varietal signatures. To further evaluate the behaviour and consistency of the identified markers, a correlation analysis was conducted between the original measured elemental concentrations and the corresponding class-specific SHAP attribution values. This analysis enabled assessment of the relationship between the contribution patterns highlighted by the explainability approach and the actual measured chemical variability in the samples.

3. Results and discussion

Results are interpreted within the framework that wheat grain composition reflects geographically structured variability in lithology-dependent Sr isotope signatures and in the bioavailable soil trace-element pool controlling soil-plant transfer processes.

Accordingly, the present study focuses on macro-area discrimination across major Italian geological domains rather than fine-scale classification within individual regions.

3.1. Multi-elemental composition of wheat samples (ICP–MS)

The Kruskal–Wallis test was applied separately to the 2023 and 2024 datasets to assess differences in elemental concentrations across the three Italian macro-areas (Northern, Central and Southern). Test statistics (H) and associated *p*-values are summarised in Table 1.

Table 1
Results of the Kruskal–Wallis test (*H* statistics and *p*-values) for elemental concentrations in wheat samples collected in 2023 and 2024, grouped according to Italian macro-areas (Northern, Central, and Southern).

	2023		2024	
Element	Parameter *H*	Test *p* value	Parameter *H*	Test *p* value
Al	0.517	0.772	1.530	0.465
As	21.082	**<0.0001**	3.227	0.199
Ba	2.989	0.224	5.383	0.068
Ca	5.768	0.056	14.958	**0.001**
Cd	9.052	**0.011**	16.344	**0.0003**
Ce	3.397	0.183	6.801	**0.033**
Co	0.594	0.743	10.037	**0.007**
Cr	4.930	0.085	6.307	**0.043**
Cu	0.431	0.806	23.136	**<0.0001**
Fe	4.524	0.104	11.565	**0.003**
Hg	12.727	**0.002**	6.518	**0.038**
La	1.166	0.558	3.127	0.209
Mn	0.777	0.678	22.468	**<0.0001**
Mo	15.874	**0.0003**	10.783	**0.005**
Ni	9.995	**0.007**	22.750	**<0.0001**
Pb	0.314	0.855	15.904	**0.0003**
Rb	7.388	**0.025**	9.124	**0.010**
Sn	16.944	**0.0002**	2.876	0.237
Sr	0.790	0.674	9.747	**0.008**
Ti	7.505	**0.023**	0.260	0.878
V	1.885	0.390	6.588	**0.037**
Zn	0.422	0.810	22.371	**<0.0001**
Zr	0.679	0.712	4.241	0.120

Exact *p*-values obtained from the Kruskal–Wallis test are reported. *p*-values <0.0001 are reported as <0.0001.

Overall, the magnitude of geographical differentiation differed markedly between harvest years, indicating that elemental fingerprints are shaped by both provenance-related signals and year-dependent environmental and agronomic variability. This behaviour is consistent with the dynamic nature of element bioavailability in agroecosystems, where pedoclimatic conditions and management practices can modulate soil–plant transfer processes.

The extent of geographical differentiation increased markedly in 2024 compared with 2023, with a substantially larger number of elements showing statistically significant differences among macro-areas. This difference suggests stronger spatial structuring of wheat elemental fingerprints in the second harvest year, whereas provenance-related signals in 2023 appear to be partially masked by year-specific environmental and agronomic variability. These results align with previous observations for other cereals and plant-based food matrices, highlighting the combined influence of geographical and interannual variability on elemental fingerprints (Bagnulo et al., 2025; Danezis & Georgiou, 2022; Nguyen et al., 2023; Tsirogiannis et al., 2023).

Several variables showed a marked increase in geographical differentiation in 2024 compared with 2023. In particular, Zn, Cu, Mn and Ni showed stronger geographical structuring in 2024, whereas Mo and Sn maintained comparatively stable discriminatory behaviour across both harvest years (Table 1). In contrast, As showed significant differences only in 2023, highlighting the limited temporal robustness of some elemental markers. These results indicate that the discriminatory strength of individual elements is strongly modulated by interannual environmental and agronomic variability, with Mo and Sn exhibiting the greatest temporal stability among the investigated discriminant variables. This pattern is also reflected in the SHAP analysis. Although the relative importance of individual predictors varied between harvest years, Zn, Cu, Mn, Ni and the $^{87}Sr/^{86}Sr$ isotopic ratio consistently ranked among the most influential contributors to geographical classification, despite modest changes in their relative ranking between harvest years. Minor differences in feature ranking between 2023 and 2024 are expected, as Random Forest assigns variable importance according to the predictive information available within each dataset (Breiman, 2001; Lundberg & Lee, 2017a, 2017b). Consequently, year-specific environmental conditions affecting element bioavailability and soil–plant transfer processes may modify the relative contribution of individual predictors without compromising the robustness of the geographical discrimination model.

Strontium, considered solely in terms of elemental concentration, showed weak and inconsistent geographical discrimination. This observation supports the widely accepted view that Sr isotopic composition represents a substantially more robust provenance tracer than elemental Sr abundance alone (Danezis & Georgiou, 2022; Liu et al., 2025; Tsirogiannis et al., 2023).

3.1.1. Pedogeochemical interpretation of Zn, Ni, Mn and Cu as discriminant variables

The SHAP analysis identified Zn, Ni, Mn and Cu among the most influential contributors to geographical classification. Although all measured elemental variables were included in the modelling workflow, Zn, Ni, Mn and Cu, together with the $^{87}Sr/^{86}Sr$ isotopic ratio, emerged among the most informative variables according to SHAP analysis and were therefore considered the principal discriminant markers. Other measured variables also contributed to model predictions but were not among the most influential variables identified by the SHAP analysis and were therefore not considered primary discriminant markers. The relevance of these elements is consistent with their well-established sensitivity to soil geochemistry and environmental conditions controlling trace-element availability in agricultural systems and their transfer to cereal grains. Although soil samples were not analysed directly in the present study, the observed variability is consistent with previously documented relationships between soil geochemistry and trace-element transfer to cereal grains reported in comparable provenance

investigations (Baize et al., 2009; Zhao et al., 2013).

Zinc availability in soils is primarily controlled by pH, carbonate content and organic matter interactions, which regulate its solubility and uptake by plants (Alloway, 2008; Broadley et al., 2007). Northern Italian cereal-growing areas are largely characterised by Alpine-derived alluvial deposits within the Po Plain basin, whereas large portions of southern Italy are dominated by carbonate platform successions associated with alkaline soil conditions (Cremaschi, 1987; Amorosi et al., 2022; Patacca & Scandone, 2007; Bosellini, 1996). Previous studies have demonstrated that Zn concentrations in wheat grains can reflect spatial variability in soil chemical properties at regional scale (Karami et al., 2009; Müller et al., 2024; Nguyen et al., 2023; Zhao et al., 2013). This interpretation is consistent with the stronger geographical differentiation observed for Zn in the 2024 dataset and supports the hypothesis that Zn may behave as a geographically informative variable under contrasting pedogeochemical conditions.

Nickel variability in soils is largely controlled by parent material and mineralogical composition (Kabata-Pendias, 2011), with elevated concentrations typically associated with mafic and ultramafic lithologies. Central Italian agricultural areas are largely associated with the heterogeneous geological framework of the Apennine chain, including sedimentary successions, flysch units and locally distributed ophiolitic complexes (Bosellini, 1996; Vai & Martini, 2001). These lithological contrasts may therefore contribute to geographically structured variability in cereal grain composition.

Manganese availability in soils is strongly regulated by redox conditions and hydrological regime, as Mn mobility increases under reducing conditions and decreases in well-aerated alkaline soils (Kabata-Pendias, 2011). Variability in drainage conditions, soil aeration and seasonal moisture availability across Italian cereal-growing environments may therefore influence Mn uptake by wheat plants.

Copper behaviour in soils is strongly influenced by interactions with organic matter and clay minerals, which regulate its retention and bioavailability in agricultural environments (Alloway, 2008).

The geographical relevance of these elements is further supported by the complex geological structure of the Italian peninsula. Alpine-derived alluvial deposits dominate the Po Plain of Northern Italy (Vai & Martini, 2001), whereas Central Italy is characterised by the heterogeneous sedimentary successions and locally distributed ophiolitic complexes of the Apennine belt (Patacca & Scandone, 2007). Southern Italy, in turn, is largely underlain by carbonate platform successions associated with Mediterranean pedoclimatic conditions (Bosellini, 1996).

Large-scale geochemical surveys of European agricultural soils further support this interpretation. In particular, the GEMAS project documented systematic continental-scale variability in Zn, Ni, Mn and Cu distributions associated with lithology, carbonate content and soil texture across European agricultural landscapes (Reimann et al., 2014). Similar conclusions have been reported in recent multi-element fingerprinting studies of cereal matrices, confirming the continued relevance of trace-element profiling as a tool for geographical authentication of wheat and other agricultural commodities (Müller et al., 2024; Nguyen et al., 2023).

Taken together, these observations suggest that the prominence of Zn, Ni, Mn and Cu is consistent with known soil–plant transfer mechanisms operating across heterogeneous geological and pedoclimatic environments such as those characterising Italian cereal-growing regions.

Although the geographical variability observed in the present study is primarily governed by pedogeochemical controls, the elemental composition of wheat grains also reflects the influence of agronomic management. Fertilisation strategies and cultivar-dependent nutrient uptake may modify the bioavailability of trace elements in soils and consequently their accumulation in plant tissues (Cakmak, 2008; White & Broadley, 2009). Likewise, soil amendments may alter trace-element mobility through changes in soil physicochemical properties (Kabata-Pendias, 2011), whereas irrigation practices may locally influence element availability by modifying soil moisture conditions and the composition of the bioavailable soil solution. Among the investigated elements, these influences are expected to be most pronounced for Zn and Cu, which are generally more responsive to agricultural inputs than to conservative geochemical processes. Zinc availability is strongly affected by soil pH and micronutrient fertilisation (Alloway, 2008), whereas Cu concentrations may additionally respond to repeated applications of Cu-based plant protection products (Schneider et al., 2019). By contrast, Mn and Ni remain more closely associated with soil redox conditions, mineralogy and parent material, although their bioavailability can still be modulated by soil chemical properties (Kabata-Pendias, 2011). Likewise, irrigation water may locally influence the bioavailable Sr pool, whereas the $^{87}Sr/^{86}Sr$ isotopic ratio is predominantly governed by the geological origin of bioavailable strontium and is transferred to plants with negligible isotopic fractionation (Bentley, 2006; Capo et al., 1998; Voerkelius et al., 2010).

Although these factors may alter the absolute concentrations of individual elements, they are expected to generate predominantly field-scale variability rather than the geographically coherent geochemical gradients observed across contrasting Italian pedological settings. Accordingly, agricultural management is more likely to contribute to within-area variability, whereas the reproducible discrimination observed among the three macro-areas is more plausibly explained by differences in geological substrate and pedogenesis. In this context, integrating multi-element fingerprints with the geologically constrained $^{87}Sr/^{86}Sr$ isotopic ratio provides a more robust framework of geographical authentication by anchoring the classification to a tracer that reflects the bioavailable Sr reservoir derived from the local geological substrate and is therefore less susceptible to local management-related variability.

3.1.2. Evaluation of potential species-related effects and interpretability of discriminant variables

To evaluate whether wheat species could confound geographical discrimination, the main SHAP-selected variables (Zn, Ni, Mn, Cu and $^{87}Sr/^{86}Sr$) were compared between *Triticum aestivum* and *Triticum durum* within each macro-area and separately for each harvest year. Species-related differences were generally limited. In 2024, significant differences were observed only for Mn and Ni in Northern Italy and for Mn in Central Italy, whereas no significant species-related differences were detected in Southern Italy or during the 2023 harvest. Overall, species-related differences were limited, geographically inconsistent and restricted to a small number of elemental variables (Table S5, Supplementary Materials).

These results indicate that the observed geographical discrimination patterns cannot be explained by species composition alone but are primarily associated with geographically structured pedogeochemical variability captured by the integrated elemental–isotopic fingerprinting framework. Overall, the magnitude and geographical consistency of species-related effects were substantially lower than those associated with macro-area discrimination. Consequently, although both wheat species were included in the dataset, species composition is unlikely to have introduced systematic bias into the geographical classification framework adopted in this study.

The agreement between the SHAP-selected variables and soil geochemical controls previously reported in the literature supports the plausibility and interpretability of the explainable machine-learning approach and indicates that the classification model captures environmentally meaningful variability rather than dataset-specific statistical relationships, consistent with recent applications of multi-element fingerprinting and interpretable machine-learning strategies in food provenance research (Müller et al., 2024; Nguyen et al., 2023).

The identification of Zn, Ni, Mn and Cu as key contributors is therefore consistent with previous studies demonstrating that wheat grain elemental composition retains a measurable imprint of soil parent material, pedoclimatic conditions and agricultural management practices (Baize et al., 2009; Müller et al., 2024; Nguyen et al., 2023; Zhao

et al., 2013), supporting their interpretation as geographically meaningful variables rather than dataset-specific statistical artefacts. More broadly, the increasing application of advanced analytical methodologies for the characterisation of food matrices reflects the growing interest in robust and reliable analytical strategies for food quality assessment and authenticity research (Ji et al., 2021; Yang et al., 2026). In the present study, these approaches were applied to investigate the geographical discrimination of Italian wheat through integrated elemental and isotopic fingerprinting. For graphical representation, a limited number of elements was selected (Zn, Ni, Mo and Cu) as representative examples of different behaviours: strong geographical discrimination (Zn), marked interannual variability (Ni), consistent secondary markers (Mo), and elements that become discriminant in specific years (Cu). This selection was intended to illustrate the diversity of elemental responses to geographical and temporal factors, rather than to represent the full elemental dataset exhaustively. Fig. 1 illustrates the distributional patterns associated with selected discriminant elements across Italian macro-areas and harvest years. The boxplots highlight the combined influence of geographical and interannual variability on elemental distributions.

The comparative heatmap based on globally z-score-normalised elemental concentrations (Fig. 2) provides a synthetic view of the joint geographical and interannual variability of wheat samples (Danezis & Georgiou, 2022; González-Domínguez et al., 2022). Because the normalisation was performed across the entire dataset (2023–2024 combined), the colour scale reflects relative enrichment and depletion with respect to the overall mean, enabling direct comparison of multi-elemental profiles across years and macro-areas.

These patterns indicate that elemental fingerprints are structured by the combined influence of geographical and interannual variability (Nguyen et al., 2023; Telloli et al., 2024; Zhao et al., 2013). In line with the univariate results (Table 1) and the selected boxplots (Fig. 1), the heatmap suggests that a subset of elements (notably Ni and Mo in both years, and Cu and Zn mainly in 2024) contributes more strongly to macro-area differentiation. In contrast, other variables appear comparatively uniform and thus less informative for geographical discrimination. A further relevant feature is the marked difference between the 2023 and 2024 blocks, with more pronounced and coherent contrasts across macro-areas in 2024. This visual pattern aligns with the higher number of statistically significant elements observed in 2024 (sixteen vs eight in 2023; Table 1), indicating a stronger spatial structuring of elemental composition in the second harvest year. Such year-to-year modulation likely reflects differences in pedoclimatic conditions and agronomic management that affect element bioavailability and plant uptake (Danezis & Georgiou, 2022; Liu et al., 2025; Telloli et al., 2024), underscoring the need to analyse samples from different harvest years to identify robust tracers.

Overall, Fig. 2 supports the concept of wheat provenance as a genuinely multivariate signature: discrimination arises from the balanced combination of multiple elements rather than from single-element extremes, reinforcing the value of integrated multi-element fingerprinting approaches in wheat traceability studies (González-Domínguez et al., 2022; Granato et al., 2018; Zhao et al., 2011).

This complex elemental structure provides a strong basis for wheat discrimination but also underscores the need to complement elemental data with more geochemically constrained and temporally stable tracers, such as the $^{87}Sr/^{86}Sr$ isotopic ratio.

3.2. Strontium isotopic signature of wheat samples (MC–ICP–MS)

Strontium isotope ratios ($^{87}Sr/^{86}Sr$) were measured in wheat samples from the 2023 and 2024 harvests to assess their suitability as geographically informative markers and to evaluate their temporal stability. Multi-elemental concentrations and isotope ratios were determined for each sample in both harvest years, ensuring consistency between the elemental and isotopic datasets.

The observed values fall within the ranges commonly reported for terrestrial ecosystems and plant-derived foodstuffs (de Caritat et al., 2022; He et al., 2025) and reflect the heterogeneous geological framework of Italian agricultural areas (Bataille & Bowen, 2012; Capo et al.,

Fig. 1. Boxplots of z-score-standardised concentrations of Cu, Mo, Ni and Zn in wheat samples, grouped by Italian macro-area (Northern, Central and Southern), for (a) 2023 and (b) 2024. Boxes represent the interquartile range (Q1–Q3), the central line indicates the median, and whiskers denote the full data range. Different letters indicate statistically significant differences among macro-areas, as identified by Dunn's post-hoc test with Bonferroni correction following the Kruskal–Wallis test ($p \leq 0.05$).

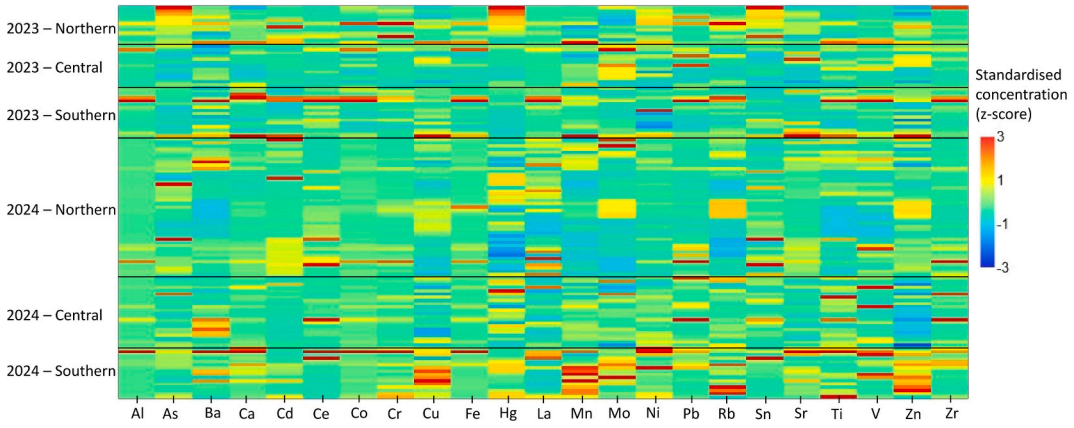

Fig. 2. Comparative heatmap of standardised elemental concentrations (z-score) in wheat samples collected in 2023 and 2024. Rows correspond to samples grouped by harvest year and geographical area, while columns represent elements. Colours indicate relative enrichment (yellow–red) or depletion (blue) relative to the overall mean of the combined dataset. (For interpretation of the references to colour in this figure legend, the reader is referred to the web version of this article.)

1998; Tommasini et al., 2018).

In the 2023 dataset, no statistically significant differences among macro-areas were detected (Kruskal–Wallis test, $p = 0.278$). Accordingly, the post-hoc Dunn test with Bonferroni correction did not reveal any significant pairwise differences, and all groups were assigned the same letter (A) in Fig. 3a. Nevertheless, median $^{87}Sr/^{86}Sr$ values suggested a consistent geographical trend, with Northern Italy showing the highest ratios, followed by Central Italy, and lower values characterising Southern Italy. This pattern is consistent with the contrasting distribution of more radiogenic siliciclastic substrates and less radiogenic carbonate-dominated domains across Italy (Bataille & Bowen, 2012; Capo et al., 1998). Where sedimentary carbonate or mafic/ultramafic igneous rocks dominate, lower $^{87}Sr/^{86}Sr$ values are generally recorded, whereas proximity to siliciclastic lithologies or metamorphic basement rocks is associated with more radiogenic signatures (de Caritat et al., 2023). The absence of statistical significance observed in 2023 therefore reflects partial overlap among distributions rather than a lack of geochemical control, indicating that the underlying lithological signal remains detectable even when interannual variability reduces statistical separation. In contrast, the 2024 dataset showed highly significant differences among macro-areas (Kruskal–Wallis test, $p < 0.0001$). This behaviour suggests that interannual differences in the statistical separation among macro-areas are likely related to year-specific variations in the relative contribution of bioavailable Sr sources rather than to changes in the underlying lithological signal controlling the isotopic baseline. The Dunn post-hoc test with Bonferroni correction separated the three groups into distinct classes (A, B and C), confirming that Northern, Central and Southern Italy were all statistically distinguishable from one another in terms of their $^{87}Sr/^{86}Sr$ signatures (Fig. 3b). On average, Central Italy had the highest median $^{87}Sr/^{86}Sr$ value, followed by Northern Italy. In contrast, Southern Italy was characterised by lower ratios. The magnitude of these differences exceeded the external reproducibility of the measurements (Section 2.4), confirming their geochemical and geographical significance.

Interannual differences were further evaluated by comparing the 2023 and 2024 datasets within each macro-area using the Mann–Whitney U test, reporting exact p-values and applying the Holm correction for multiple testing. This analysis revealed statistically significant differences between years in Central and Southern Italy, whereas no significant interannual variation was observed in Northern Italy. However, these variations were moderate and did not alter the overall isotopic ranges or the persistence of the north–centre–south gradient across years. Therefore, the greater temporal stability of the $^{87}Sr/^{86}Sr$ ratio should be interpreted relative to the more pronounced interannual variability observed for several elemental concentrations. These results indicate that, while the overall isotopic distributions remain comparable between years, moderate year-to-year variability may occur locally, particularly in Central and Southern Italy. Such

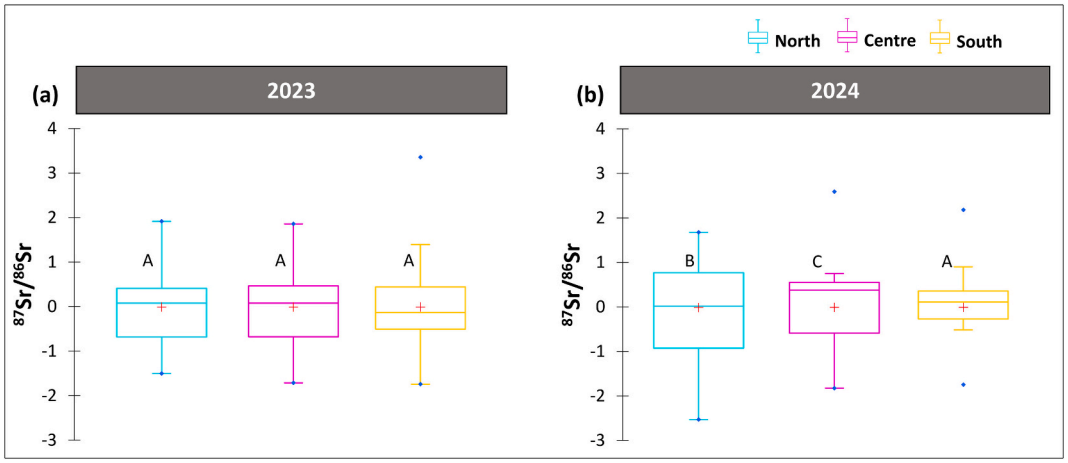

Fig. 3. Distribution of $^{87}Sr/^{86}Sr$ isotope ratios in wheat samples collected in (a) 2023 and (b) 2024, grouped by macro-area (Northern, Central and Southern Italy). Boxes represent the interquartile range (Q1–Q3), the horizontal line indicates the median, and whiskers show the minimum and maximum values. Different letters indicate statistically significant differences among groups (Kruskal–Wallis test with Dunn's post hoc test and Bonferroni correction, $p < 0.05$).

variability may reflect subtle changes in the relative contribution of bioavailable strontium from soils and irrigation waters, influenced by seasonal hydrological conditions and soil-water interactions (Bataille & Bowen, 2012; Voerkelius et al., 2010). Although species composition differed between harvest years, previous studies indicate that plant physiological differences generally have a limited influence on $^{87}Sr/^{86}Sr$ ratios compared with the dominant control exerted by the isotopic composition of the bioavailable soil strontium pool (Bentley, 2006; Capo et al., 1998; Voerkelius et al., 2010).

Despite these local interannual differences, the overall isotopic ranges and median values were remarkably similar between 2023 and 2024, highlighting the temporal robustness of the $^{87}Sr/^{86}Sr$ ratio at the national scale. This behaviour contrasts with the more pronounced year-to-year fluctuations observed for several elemental concentrations (Section 3.1), confirming the suitability of strontium isotopes as stable tracers for food authentication (Wang et al., 2025-2026; Horek Horacek et al., 2022). The persistence of a coherent north-centre-south gradient across harvest years further supports the resilience of the isotopic signals to short-term environmental perturbations, representing a major advantage for food authentication and geographical traceability applications, where consistency across harvest years is essential (He et al., 2025).

Although partial overlap among macro-areas is expected due to the complexity of Italian geology and the integration of Sr from soil and water sources during plant uptake (He et al., 2025), the results show that the $^{87}Sr/^{86}Sr$ isotopic signature retains a clear geochemical imprint of the underlying lithological background, with variable but reproducible discriminatory power between years. The $^{87}Sr/^{86}Sr$ ratio measured in wheat grains reflects the composition of the bioavailable soil strontium pool rather than bulk lithological compositions alone. This pool integrates contributions from bedrock weathering, soil exchangeable fractions and locally available irrigation waters supplying dissolved strontium to the root-accessible fraction and is transferred to plants with negligible isotopic fractionation (Bentley, 2006; Capo et al., 1998). Although soil isotopic compositions were not directly measured in the present study, the observed macro-area variability is consistent with previously documented soil-plant transfer mechanisms controlling strontium isotope signatures in agricultural products and supports the interpretation of the isotopic signal within a provenance-oriented multi-elemental and isotopic fingerprinting framework (Bentley, 2006; Capo et al., 1998; Saar de Almeida et al., 2023; Voerkelius et al., 2010). When combined with multi-elemental data, the geochemically driven and temporally robust nature of the $^{87}Sr/^{86}Sr$ ratio is likely to improve the performance and reliability of subsequent multivariate and machine learning-based classification models (Hao et al., 2021; Won et al., 2021).

Overall, these findings highlight the suitability of the $^{87}Sr/^{86}Sr$ ratio as a robust marker for wheat traceability and authentication across harvest years (Wang et al., 2025-2026; Horek Horacek et al., 2022), in line with the principle that Sr isotope ratios in agricultural products mirror the isotopic composition of bioavailable strontium in soils without significant isotopic fractionation during plant uptake (Saar de Almeida et al., 2023).

3.3. Complementarity between Sr concentration and $^{87}Sr/^{86}Sr$

A comparison of Sr concentrations measured by ICP–MS and $^{87}Sr/^{86}Sr$ isotope ratios obtained via MC–ICP–MS revealed only a weak or negligible correlation between these parameters (Fig. 4). This observation is consistent with previous research on crops and plant systems, which demonstrated that Sr isotopic composition is largely independent of total Sr content due to distinct geochemical and physiological factors influencing each variable (Bacher et al., 2023; Wang et al., 2025-2026).

The absence of a clear linear relationship in Fig. 4 indicates that information derived from elemental abundances and isotopic composition is complementary rather than redundant.

Although Sr concentrations varied substantially among harvest years and between individual samples, the $^{87}Sr/^{86}Sr$ ratios remained within a relatively narrow range. This pattern reflects distinct mechanisms governing element accumulation and isotopic composition in wheat. Sr concentrations are influenced by soil availability, agricultural practices, and environmental factors, whereas the isotopic ratio primarily reflects the geological substrate of the cultivation site. The decoupling observed here therefore enables the separation of environmentally modulated variability from lithologically controlled provenance signals within the same chemical framework. This separation provides a mechanistic basis for integrating elemental Sr concentrations and $^{87}Sr/^{86}Sr$ isotopic ratios in provenance studies, as each variable captures complementary dimensions of the soil-plant system (Capo et al., 1998; Saar de Almeida et al., 2023). In multivariate contexts, such complementarity increases model robustness by reducing the risk that classification relies disproportionately on environmentally unstable predictors.

The combined use of these variables in multivariate and machine learning models improves geographical discrimination and increases the overall reliability of predictive models (Bacher et al., 2023; Wang et al., 2025-2026).

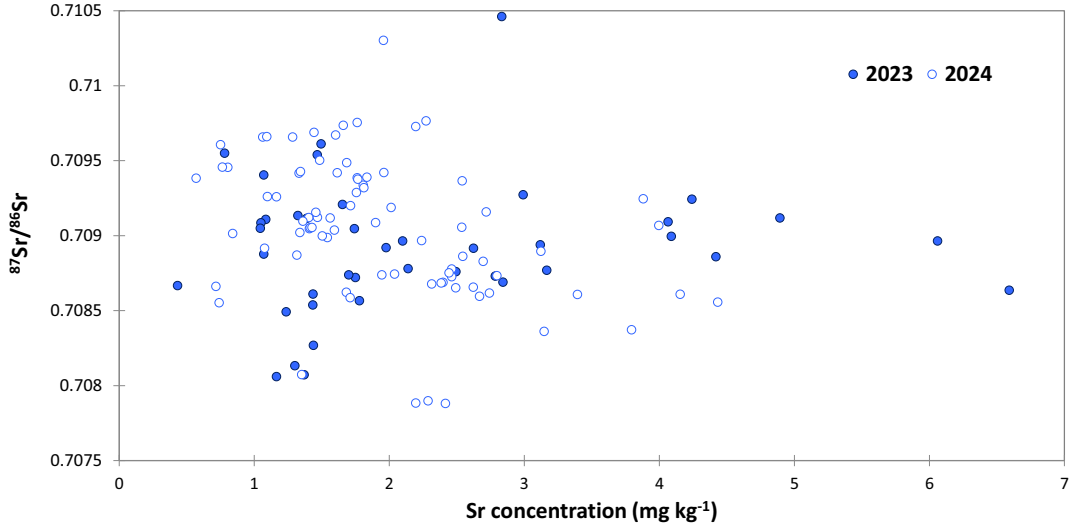

Fig. 4. Scatter plot illustrating the relationship between Sr concentration determined by ICP–MS and $^{87}Sr/^{86}Sr$ isotope ratios measured by MC–ICP–MS in wheat samples collected in 2023 and 2024.

3.4. Exploratory multivariate analysis (PCA)

Principal Component Analysis (PCA) was used as an unsupervised exploratory tool to investigate the multivariate structure of the elemental dataset and to visualise both geographical and interannual patterns in wheat samples (Jolliffe & Cadima, 2016). PCA score plots of PC1 versus PC2 for the 2023 and 2024 datasets are shown in Fig. 5.

In both harvest years, the first two principal components explained 51.1% (2023) and 46.6% (2024) of the total variance (Table S6, Supplementary Materials). The corresponding score plots reveal a partial geographical separation of samples, with wheat from Northern, Central, and Southern Italy clustering in different regions of the multivariate space. However, a clear overlap among macro-areas persists, particularly along PC2. This residual overlap confirms that linear combinations of elemental variables capture only part of geographical structure, especially when interannual variability contributes substantially to total variance. Although the PCA plots showed only partial separation among the three geographical macro-areas, this observation is not inconsistent with the high classification performance achieved by the Random Forest model. PCA is an unsupervised dimensionality reduction technique that maximizes the overall variance of the dataset without considering class membership. Consequently, the principal components explaining the largest proportion of variance do not necessarily correspond to the combinations of variables that best discriminate geographical origin. By contrast, Random Forest is a supervised learning algorithm that exploits class information to identify complex and potentially nonlinear relationships among elemental and isotopic variables. Therefore, discriminative information that is not fully captured by the first principal components can still be effectively exploited by the machine-learning model.

The 2024 dataset shows a more distinct spatial organisation, consistent with the stronger geographical differences observed in the univariate analysis (Section 3.1). Inspection of the loading coefficients (Table S7, Supplementary Materials) indicates that elements previously identified as discriminant, including Ni, Mo, Cu and Zn, contribute substantially to the variance captured by the principal components. For visual clarity, axis limits were adjusted to emphasise the main distribution of samples, while extreme scores were retained in the analysis.

Overall, PCA highlights geographically structured variation in the elemental data while underscoring the intrinsic limitations of linear, unsupervised methods (Zhao et al., 2013). These findings further justify the subsequent application of supervised and non-linear machine-learning models for geographical classification.

3.5. Machine learning classification

The results of the machine learning analyses are presented below, including the preliminary feature selection step and the subsequent classification performance for the macro-area of origin.

Multicollinearity among elemental and isotopic predictors was first assessed using the Variance Inflation Factor (VIF). An iterative VIF-based feature selection procedure was applied separately to the 2023, 2024, and combined (2023–2024) datasets to remove highly correlated variables and improve model stability. The variables excluded varied slightly across modelling scenarios. In the combined dataset (2023–2024), Co and Al were removed. In the 2024 dataset, Co, Al, Ce, and Fe were excluded, whereas in the 2023 dataset, La, Al, Hg, Ce, Cu, and Co were filtered out according to VIF criteria. This dataset-specific

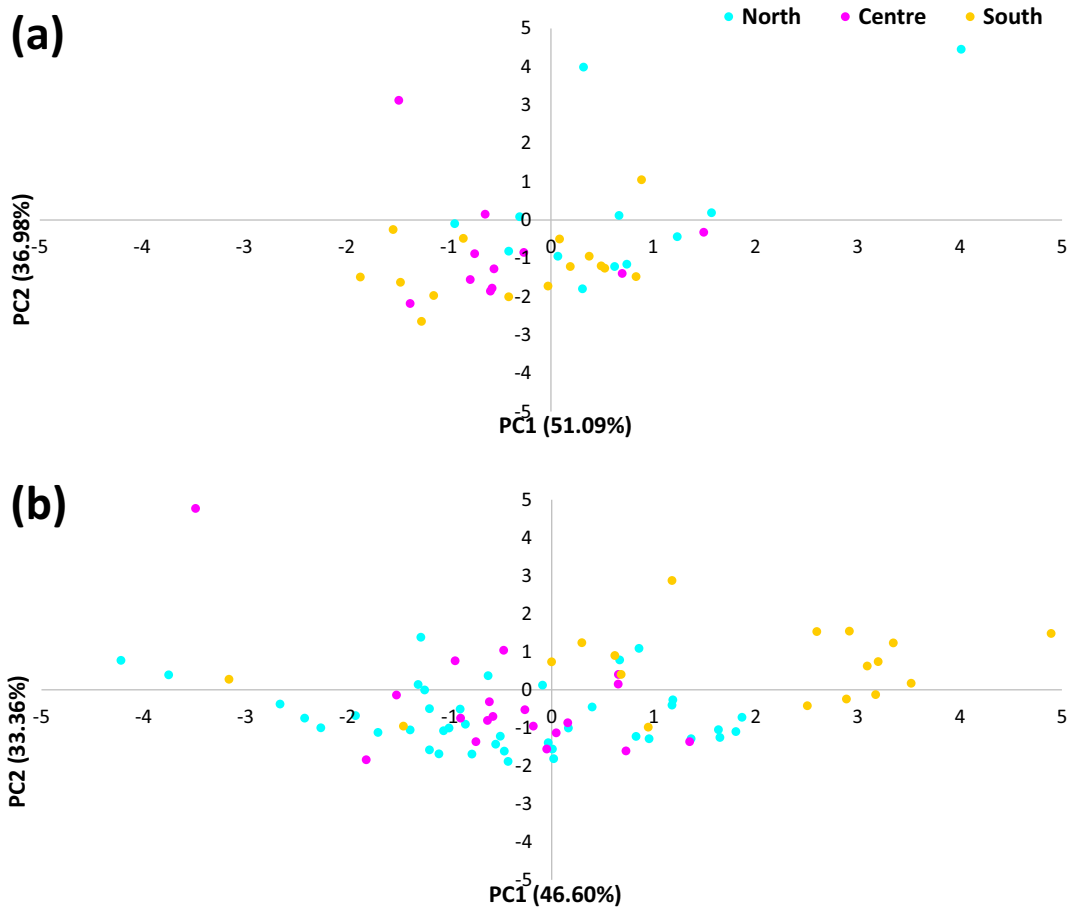

Fig. 5. PCA score plots (PC1 vs PC2) of z-score-standardised elemental concentrations in wheat samples collected in (a) 2023 and (b) 2024, grouped by macro-area (Northern, Central and Southern Italy).

filtering yielded reduced, less redundant predictor sets, thereby improving the numerical stability of the classification models. This step was particularly important given the moderate sample size and the intrinsic correlations among geochemically related elements, which could otherwise inflate model variance and compromise generalisation.

Random Forest classifiers were subsequently developed to predict the macro-area of origin. Model performance was evaluated using a repeated k-fold cross-validation framework, and classification metrics were calculated under a multi-class evaluation strategy. The results are summarised in Table 2 and reported as mean ± standard deviation across 10-fold cross-validation repeated 20 times.

For the 2023 dataset, the Random Forest model achieved a mean accuracy of 0.75 ± 0.08, a F1-score of 0.73 ± 0.09, and a recall of 0.73 ± 0.08. Specificity was higher (0.86 ± 0.04), indicating a stronger ability to correctly identify samples that do not belong to the target class. In the 2024 dataset, classification performance improved, reaching a mean accuracy of 0.81 ± 0.06. The macro F1-score and recall were 0.77 ± 0.08 and 0.74 ± 0.08, respectively, while specificity remained high at 0.87 ± 0.04. Confusion matrices for both datasets are reported in the Supplementary Information (Figs. S1–S2) and provide additional insight into class-wise performance and misclassification patterns, supporting the trends observed in the overall accuracy and recall metrics. This improved performance aligns with the stronger geographical differentiation observed in 2024 in both the elemental (Section 3.1) and isotopic (Section 3.2) datasets.

Receiver Operating Characteristic (ROC) curves were computed under a one-vs-rest scheme to further evaluate class-wise discriminative performance. For both datasets, the model shows strong separability across all three geographical classes, with high AUC values and relatively low variability across cross-validation folds. In the 2023 dataset in Supplementary Fig. 3, the Northern class exhibits the highest discriminative performance (AUC = 0.97 ± 0.04), followed by the Central (AUC = 0.91 ± 0.05) and Southern classes (AUC = 0.85 ± 0.08), with an overall macro-average AUC of 0.90 ± 0.04. A similar pattern is observed in the 2024 dataset represented in Supplementary Fig. 4, where all classes show consistently high AUC values (Northern: 0.95 ± 0.03; Central: 0.93 ± 0.06; Southern: 0.97 ± 0.02), resulting in an overall macro-average AUC of 0.94 ± 0.03. These results indicate that, despite the moderate multi-class accuracy, the model achieves strong class-wise discrimination, confirming the presence of a robust geographical signal when evaluated in a one-vs-rest framework. When the two harvest years were combined (2023–2024), intermediate performance values were observed, with a mean accuracy of 0.74 ± 0.05, an F1-score of 0.72 ± 0.06, and a sensitivity of 0.71 ± 0.06. Specificity remained stable (0.85 ± 0.03), indicating consistent classification behaviour across modelling scenarios and supporting the complementary contribution of elemental and isotopic variables to geographical discrimination. The slightly lower performance observed in the combined dataset likely reflects the additional interannual variability introduced when pooling harvest years, which increases within-class heterogeneity while better approximating real-world authentication scenarios.

Across all datasets, specificity consistently exceeded sensitivity, indicating that the model was more stable in correctly identifying non-target classes within the three-class classification framework. This asymmetry suggests that misclassifications are primarily associated with partial overlap among macro-areas, rather than with systematic model bias. Importantly, the observed performance should be interpreted in the context of the intrinsic complexity of the classification task, which involves a broad geographical scale (Northern, Central, and Southern Italy) and heterogeneous sample composition, including two wheat species (*T. aestivum* L. and *T. durum Desf.*). Both factors contribute to increased chemical variability and reduced class separability. Within this realistic and challenging framework, classification accuracies in the range of 0.76–0.81 indicate a consistent and practically meaningful level of geographical discrimination.

The analytical precision achieved for both ICP–MS and MC–ICP–MS measurements was considered adequate to support the robustness of the geographical discrimination and classification results.

Table 2
Classification performance of the Random Forest model for geographical origin prediction in the 2023 and 2024 harvest years and in the combined dataset (2023–2024). Results are expressed as mean ± standard deviation of Accuracy, F1-score, Precision, Recall and Specificity, computed across 20 repetitions of a k-fold cross-validation procedure.

Metric	2023 Dataset	2024 Dataset
Accuracy	0.75 ± 0.08	0.81 ± 0.06
F1-score	0.73 ± 0.09	0.77 ± 0.08
Precision	0.79 ± 0.09	0.87 ± 0.06
Recall	0.73 ± 0.08	0.74 ± 0.08
Specificity	0.86 ± 0.04	0.87 ± 0.04
AUC-ROC	0.91 ± 0.04	0.95 ± 0.03

3.6. Explainable artificial intelligence (SHAP) analysis

To enhance model interpretability and provide a chemically meaningful interpretation of the classification results, an explainable artificial intelligence (XAI) approach based on SHapley Additive exPlanations (SHAP) was integrated into the workflow (Lundberg et al., 2020; Lundberg & Lee, 2017a, 2017b). Class-specific SHAP summary plots for the 2023 and 2024 datasets are presented in Fig. 6a,b,c and Fig. 6d,e,f, respectively, while SHAP results for the combined dataset (2023–2024) are provided in the Supplementary Materials (Fig. S5).

In the 2023 dataset (Fig. 6a,b,c), discrimination among macro-areas was driven by a combination of trace elements and the $^{87}Sr/^{86}Sr$ isotopic ratio. The contributions of individual variables were relatively evenly distributed, with several elements showing moderate, class-dependent influence on model predictions. This pattern reflects the more limited geographical structuring observed in the 2023 univariate and PCA analyses.

In contrast, the 2024 dataset (Fig. 6d,e,f) showed a clearer hierarchy of influential predictors. In particular, the $^{87}Sr/^{86}Sr$ isotopic ratio emerged as one of the most influential variables across macro-areas, alongside selected trace elements such as Zn, Mn, Ni, and Cu. The stronger and more consistent SHAP contributions observed in 2024 align with the higher classification performance achieved in this year and with the more pronounced geographical differentiation highlighted in Sections 3.1 and 3.2.

The SHAP analysis further confirms that classification does not rely on single dominant variables but rather on the cumulative contribution of multiple predictors, each encoding different aspects of the soil–plant–environment system.

The pooled SHAP results (Fig. S5) further confirm that wheat provenance is determined by a multivariate chemical signature rather than by single-element effects. Although certain variables exhibit class-specific dominance, the overall classification behaviour arises from the combined contributions of multiple elemental and isotopic predictors. In the combined dataset (2023–2024), the $^{87}Sr/^{86}Sr$ isotopic ratio consistently appears among the top-ranked predictors across macro-areas, further supporting its robustness as a temporally stable and geochemically meaningful tracer within the multivariate framework.

The results obtained in the present study are consistent with previous investigations demonstrating the usefulness of multi-elemental fingerprinting and strontium isotope ratios for wheat provenance discrimination at regional scales (Bacher et al., 2023; Zhao et al., 2013). However, most earlier studies relied on single-year datasets and conventional chemometric classification approaches, whereas the present work integrates multi-elemental and isotopic information across two harvest years and applies explainable machine-learning methods to interpret the environmental drivers of geographical discrimination. This combined approach improves both the robustness and interpretability of provenance classification by explicitly linking model-derived feature

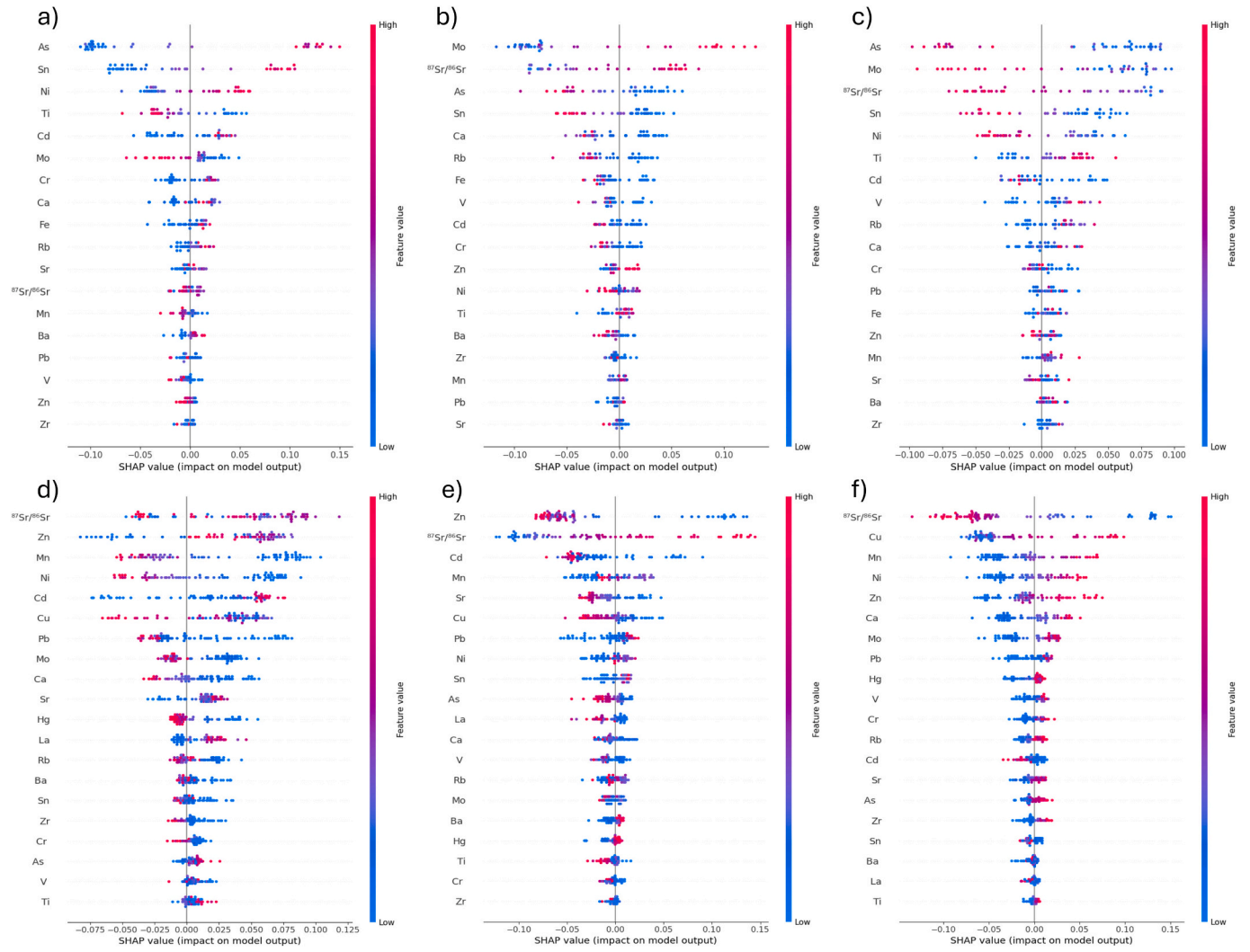

Fig. 6. Class-specific SHAP summary plots for the Random Forest model applied to the (a,b,c) 2023 and (d,e,f) 2024 datasets, illustrating the relative contribution of elemental concentrations and the $^{87}Sr/^{86}Sr$ isotopic ratio to geographical classification.

importance with established lithology-soil-plant transfer mechanisms controlling wheat grain composition, thereby supporting a process-informed interpretation of geographical traceability signals rather than a purely empirical classification outcome.

Overall, the SHAP analysis links statistical relevance to geochemical plausibility, indicating that the predictive structure of the model reflects chemically interpretable patterns rather than spurious correlations. A more detailed pedogeochemical interpretation of the main SHAP-selected variables (Zn, Ni, Mn and Cu) is provided in Section 3.1, where their contribution is discussed in relation to soil geochemistry, regional geological variability and known soil-plant transfer processes. This consistency between SHAP-derived feature importance and established soil-plant transfer mechanisms further supports the hypothesis that geographically structured soil geochemistry is recorded in wheat grain composition and captured by the explainable machine-learning framework applied in this study.

3.7. Limitations

Despite the promising results obtained in this study, several limitations should be acknowledged. First, the dataset size is relatively limited, which constrains the possibility of defining a fully independent external validation dataset. As a consequence, model performance was evaluated using repeated k-fold cross-validation, which provides a robust internal validation strategy but does not fully demonstrate generalizability to completely unseen samples. Future studies should therefore include independent validation datasets collected from additional regions, cultivars and production environments to verify the robustness, transferability and practical applicability of the proposed elemental–isotopic authentication framework under real-world conditions.

In addition, pronounced interannual variability in elemental composition was observed between the 2023 and 2024 datasets. This variability reflects a clear distributional shift (domain shift) between years, likely driven by differences in environmental conditions and agronomic factors. For this reason, the two datasets were analysed independently, and no cross-year validation was performed. While this approach ensures internally consistent modelling, it also implies that the current results are primarily representative of within-year geographical discrimination, rather than two different years model transferability. Differences in sample size and species composition between the two harvest years may represent an additional source of variability.

An additional limitation concerns the imbalance in sample distribution among macro-areas, particularly in the 2024 dataset, where Northern Italy was represented by a larger number of samples than Central and Southern Italy. This imbalance reflects the availability of samples within the study design and may have influenced class representation during model training. Model evaluation was performed using

repeated k-fold cross-validation; however, no specific stratification procedure was applied to preserve class proportions across folds. Similarly, no additional class-weighting strategy was implemented, as the degree of class imbalance was considered moderate and preliminary analyses did not indicate substantial performance degradation for the underrepresented classes. Nevertheless, some bias related to uneven class representation cannot be completely excluded. Future studies should aim to achieve a more balanced sampling design and evaluate stratified resampling or class-weighting approaches to further strengthen model robustness and class-wise comparability.

The 2023 dataset includes both common and durum wheat, whereas the 2024 dataset is dominated by durum wheat. Although species was not explicitly included as a classification variable, a potential confounding effect between species and geographical origin cannot be entirely excluded, as different wheat types may be unevenly distributed across regions. Furthermore, the classification task involves a broad geographical scale (Northern, Central, and Southern Italy) and heterogeneous sample composition, introducing variability related to environmental, geological, and agronomic factors. This intrinsic complexity may reduce class separability and affect predictive performance. Finally, feature selection based on variance inflation factor (VIF) was applied independently to each dataset to address collinearity. However, differences in the correlation structure between years led to partially different feature sets being selected, which may contribute to variability in model interpretation (e.g., SHAP rankings) across datasets. Future work will focus on expanding the dataset across years and regions, enabling the development of different years calibrated models and the construction of independent external validation datasets to better assess model robustness under realistic conditions. Future developments should also evaluate simplified analytical workflows and reduced-variable models to improve operational applicability while maintaining satisfactory classification performance.

4. Conclusions

This study presents an integrated analytical framework combining multi-elemental profiling (ICP–MS), strontium isotopic fingerprinting (MC–ICP–MS) and SHAP-based explainable machine-learning approaches for assessing the geographical origin of Italian wheat in different years. The joint use of elemental and isotopic data provided complementary chemical information, reflecting both environmentally driven variability and geochemically controlled provenance signals.

Multi-elemental composition showed marked interannual variability and variable geographical discrimination, whereas the $^{87}Sr/^{86}Sr$ isotopic ratio exhibited greater temporal stability and a clearer link to the geological background (Stantis et al., 2026). The persistence of coherent isotopic patterns across harvest years highlights the resilience of the Sr isotopic signal to short-term environmental fluctuations, confirming its suitability as a geographically informative tracer (Bacher et al., 2023).

Integrating elemental and isotopic datasets improved classification performance and enabled discrimination among Italian macro-areas. Random Forest model combined with SHAP-based analysis enhanced model interpretability by identifying the key chemical drivers of geographical classification. Additional intra-area comparisons between wheat species confirmed that species-related compositional variability was limited and not consistent between the two different years and macro-areas, supporting the interpretation that geographical discrimination was mainly driven by pedogeochemical rather than species-related effects.

Overall, wheat geographical origin is more reliably characterised by the combined contribution of elemental and isotopic signatures interpreted through explainable machine-learning approaches than by individual markers considered separately.

The originality of the proposed framework lies in the process-informed integration of ICP–MS multi-elemental profiling, MC–ICP–MS strontium isotopic fingerprinting and SHAP-based explainable machine learning enabling interpretation of geographical variability in relation to lithology and soil-related controls previously discussed in the literature, rather than relying on purely empirical classification models. This approach links classification performance with geochemically meaningful soil–plant transfer processes controlling elemental mobility and isotopic variability across contrasting geological domains. Further application of the model to future harvest years and the inclusion of larger and more geographically diverse datasets will strengthen its robustness and operational applicability. The proposed framework could support regulatory traceability and authenticity assessment by providing an objective, data-driven approach for wheat origin verification. Moreover, the integration of multi-elemental and isotopic fingerprinting with explainable artificial intelligence offers a transparent and scientifically interpretable tool for PDO/PGI verification and routine authenticity monitoring, supporting fraud prevention and strengthening consumer confidence in geographical labeling.

CRediT authorship contribution statement

Giulia Puzo: Writing – review & editing, Writing – original draft, Visualization, Validation, Investigation, Data curation, Conceptualization. **Tea Zuliani:** Writing – review & editing, Methodology, Investigation, Data curation. **Michele Magarelli:** Writing – review & editing, Visualization, Software, Investigation, Formal analysis. **Pierfrancesco Novielli:** Writing – review & editing, Software, Investigation, Formal analysis. **Emilia Pucci:** Writing – review & editing, Investigation, Data curation. **Valeria Poscente:** Writing – review & editing, Investigation, Data curation. **Alessandra Bernardini:** Writing – review & editing, Investigation, Data curation. **Sabina Tangaro:** Writing – review & editing, Validation, Supervision, Methodology, Formal analysis. **Massimo Reverberi:** Writing – review & editing, Supervision, Funding acquisition, Conceptualization. **Claudia Zoani:** Writing – review & editing, Validation, Supervision, Methodology, Funding acquisition, Conceptualization.

Funding sources

This paper is funded by METROFOOD-IT project funding from the European Union – NextGenerationEU, NRRP-Mission 4 ‘Education and Research’ Component 2: from research to business, Investment 3.1: Fund for the realisation of an integrated system of research and innovation infrastructures [IR0000033] (D.M. Prot. n.120 del 21/06/2022) and by AGRITECH funding from the European Union-NextGenerationEU, NRRP-Mission 4 ‘Education and Research’ Component 2: from research to business, Investment 1.4: ‘National Research Centre for Agricultural Technologies’ Agritech CUP HUB – B63D21015240004.

Declaration of competing interest

The authors declare the following financial interests/personal relationships which may be considered as potential competing interests: Dr. Claudia Zoani is Guest Editor of the Special Issue in which this article is published. Given her role as Guest Editor, Dr. Claudia Zoani had no involvement in the peer-review of this article and has no access to information regarding its peer-review. The remaining authors declare that they have no known competing financial interests or personal relationships that could have appeared to influence the work reported in this paper. If there are other authors, they declare that they have no known competing financial interests or personal relationships that could have appeared to influence the work reported in this paper.

Appendix A. Supplementary data

Supplementary data to this article can be found online at https://doi.org/10.1016/j.foodchem.2026.150491.

Data availability

Data will be made available on request.

References

Adadi, A., & Berrada, M. (2018). Peeking inside the black-box: A survey on explainable artificial intelligence (XAI). *IEEE Access, 6*, 52138–52160. https://doi.org/10.1109/ACCESS.2018.2870052

Alloway, B. J. (2008). *Zinc in soils and crop nutrition* (2nd ed.). International Zinc Association & International Fertilizer Industry Association.

Alves, L. R., dos Reis, A. R., & Gratão, P. L. (2016). Heavy metals in agricultural soils: From plants to our daily life (a review). *Científica, 44*(3), 346–361. https://doi.org/10.15361/1984-5529.2016v44n3p346-361

Amorosi, A., Sammartino, I., Dinelli, E., Campo, B., Guercia, T., Trincardi, F., & Pellegrini, C. (2022). Provenance and sediment dispersal in the Po–Adriatic source-to-sink system unraveled by bulk-sediment geochemistry and its linkage to catchment geology. *Earth-Science Reviews, 234*, Article 104202. https://doi.org/10.1016/j.earscirev.2022.104202

Bacher, F., Aguzzoni, A., Chizzali, S., Pignotti, E., Puntscher, H., Zignale, P., Voto, G., Tagliavini, M., Tirler, W., & Robatscher, P. (2023). Geographic tracing of cereals from South Tyrol (Italy) and neighboring regions via $^{87}Sr/^{86}Sr$ isotope analysis. *Food Chemistry, 405*(Pt B), Article 134890. https://doi.org/10.1016/j.foodchem.2022.134890

Bagnulo, E., Felizzato, G., Caratti, A., Bortolini, C., Cordero, C., Bicchi, C., & Liberto, E. (2025). Machine learning models for terroir classification and blend similarity prediction: A proof-of-concept to enhance cocoa quality evaluation. *Food Chemistry*. https://doi.org/10.1016/j.foodchem.2025.144620

Baize, D., Bellanger, L., & Tomassone, R. (2009). Relationships between concentrations of trace metals in wheat grains and soil. *Agronomy for Sustainable Development, 29*(2), 297–312. https://doi.org/10.1051/agro:2008057

Bataille, C. P., & Bowen, G. J. (2012). Mapping $^{87}Sr/^{86}Sr$ variations in bedrock and water for large-scale provenance studies. Chemical Geology, 304–305, 39–52 https://doi.org/10.1016/j.chemgeo.2012.01.028.

Bentley, R. A. (2006). Strontium isotopes from the earth to the archaeological skeleton: A review. *Journal of Archaeological Method and Theory, 13*(3), 135–187. https://doi.org/10.1007/s10816-006-9009-x

Bosellini, A. (1996). *Geologia delle Dolomiti*. Athesia.

Breiman, L. (2001). Random forests. *Machine Learning, 45*(1), 5–32. https://doi.org/10.1023/A:1010933404324

Broadley, M. R., White, P. J., Hammond, J. P., Zelko, I., & Lux, A. (2007). Zinc in plants. *New Phytologist, 173*(4), 677–702. https://doi.org/10.1111/j.1469-8137.2007.01996.x

Buyuktepe, O., Catal, C., Kar, G., Bouzembrak, Y., Marvin, H., & Gavai, A. (2023). Food fraud detection using explainable artificial intelligence. *Expert Systems, 42*(1), Article e13387. https://doi.org/10.1111/exsy.13387

Cakmak, I. (2008). Enrichment of cereal grains with zinc: Agronomic or genetic biofortification? *Plant and Soil, 302*(1–2), 1–17. https://doi.org/10.1007/s11104-007-9466-3

Capo, R. C., Stewart, B. W., & Chadwick, O. A. (1998). Strontium isotopes as tracers of ecosystem processes: Theory and methods. *Geoderma, 82*(1–3), 197–225. https://doi.org/10.1016/S0016-7061(97)00102-X

de Caritat, P., Dosseto, A., & Dux, F. (2022). A strontium isoscape of inland southeastern Australia. *Earth System Science Data, 14*, 4022–4271. https://doi.org/10.5194/essd-14-4271-2022

de Caritat, P., Dosseto, A., & Dux, F. (2023). A strontium isoscape of northern Australia. *Earth System Science Data, 15*, 1655–2023 1673. https://doi.org/10.5194/essd-15-1655-2023

Coelho, I., Matos, A. S., Epova, E. N., Barre, J., Cellier, R., Ogrinc, N., … Donard, O. F. X. (2023). Multi-element and multi-isotopic profiles of port and Douro wines as tracers for authenticity. *Journal of Food Composition and Analysis, 115*, Article 104988. https://doi.org/10.1016/j.jfca.2022.104988

Danezis, G. P., & Georgiou, C. A. (2022). Elemental metabolomics: Food elemental assessment could reveal geographical origin. *Current Opinion in Food Science, 44*, Article 100812. https://doi.org/10.1016/j.cofs.2022.100812

Durante, C., Bertacchini, L., Bontempo, L., Camin, F., Manzini, D., & Versari, A. (2013). Geographical traceability based on $^{87}Sr/^{86}Sr$ indicator: A first approach for PDO Lambrusco wines from Modena. *Food Chemistry, 141*(3), 2779–2787. https://doi.org/10.1016/j.foodchem.2013.05.108

Food and Agriculture Organization of the United Nations. (2023). *Wheat production and trade statistics [Dataset]*. FAOSTAT. Retrieved January 20, 2023, from https://www.fao.org/faostat/.

Furdek Turk, M., Epova, E. N., Pošćić, F., Nasr, E., Barre, J., Donard, O. F. X., & Zuliani, T. (2022). Determination of 87Sr/86Sr isotopic ratio in olive oil and pomace using multicollector-ICPMS: Analysis of pomace residues as a simpler approach for determination of 87Sr/86Sr ratio in olive oil with low Sr content. *Journal of Food Composition and Analysis, 112*, Article 104675. https://doi.org/10.1016/j.jfca.2022.104675

González-Domínguez, R., Sayago, A., & Fernández-Recamales, Á. (2022). An overview on the application of Chemometrics tools in food authenticity and traceability. *Foods, 11*(23), 3940. https://doi.org/10.3390/foods11233940

Granato, D., Putnik, P., Bursać Kovačević, D., Sousa Santos, J., Calado, V., Rocha, R. S., … Pomerantsev, A. (2018). Trends in chemometrics: Food authentication, microbiology, and effects of processing. *Comprehensive Reviews in Food Science and Food Safety, 17*(3), 663–677. https://doi.org/10.1111/1541-4337.12341

Hao, X., Gao, F., Wu, H., Song, Y., Liang, Z., Li, H., & Wang, H. (2021). From soil to grape and wine: Geographical variations in elemental profiles in different Chinese regions. *Foods, 10*(12), 3108. https://doi.org/10.3390/foods10123108

Hassoun, A., Kamiloglu, S., Garcia-Garcia, G., Parra-López, C., Trollman, H., Jagtap, S., … Esatbeyoglu, T. (2023). Implementation of relevant fourth industrial revolution innovations across the supply chain of fruits and vegetables: A short update on traceability 4.0. *Food Chemistry, 409*, Article 135303. https://doi.org/10.1016/j.foodchem.2022.135303

He, J., Han, X., Jiang, Y., Ren, A., Yang, Z., Zhang, Z., Wang, M., Yang, B., Yin, M., Peng, H., & Huang, L. (2025). Study on strontium isotope characteristics in plants: Providing reference for food production area traceability. *Journal of Agricultural and Food Chemistry, 73*(33), 20745–20755. https://doi.org/10.1021/acs.jafc.5c05277

Horek Horacek, M., Klová, L., Hudcovicová, M., Ondreičková, K., Gubiš, J., & Hölzl, S. (2022). Differentiation of apricots of different geographic origin in central and southern Europe by applying $^{87}Sr/^{86}Sr$ analysis: Potential and limitations. *Foods, 11*(15), 2239. https://doi.org/10.3390/foods11152239

Ji, X., Yin, M., Hao, L., Shi, M., Liu, H., & Liu, Y. (2021). Effect of inulin on pasting, thermal, rheological properties and in vitro digestibility of pea starch gel. *International Journal of Biological Macromolecules, 193*(Part B), 1669–1675. https://doi.org/10.1016/j.ijbiomac.2021.11.004

Jolliffe, I. T., & Cadima, J. (2016). Principal component analysis: A review and recent developments. *Philosophical Transactions of the Royal Society A: Mathematical, Physical and Engineering Sciences, 374*(2065), 20150202. https://doi.org/10.1098/rsta.2015.0202

Kabata-Pendias, A. (2011). *Trace elements in soils and plants* (4th ed.). CRC Press.

Karami, M., Afyuni, M., Rezainejad, Y., Schulin, R., & Keller, A. (2009). Heavy metal uptake by wheat from a sewage sludge-amended calcareous soil. *Nutrient Cycling in Agroecosystems, 83*(1), 51–61. https://doi.org/10.1007/s10705-008-9198-7

Liu, X., Fan, K., Lu, Y., Rao, Q., Zhang, Q., Geng, H., … Song, W. (2025). Multivariate fusion for identification of geographic origins and varieties of coix seed. *npj Science of Food, 9*(1), 41. https://doi.org/10.1038/s41538-025-00389-9

Lundberg, S. M., Erion, G., Chen, H., DeGrave, A., Prutkin, J. M., Nair, B., … Lee, S. I. (2020). From local explanations to global understanding with explainable AI for trees. *Nature Machine Intelligence, 2*(1), 56–67. https://doi.org/10.1038/s42256-019-0138-9

Lundberg, S. M., & Lee, S.-I. (2017a). A unified approach to interpreting model predictions. In *Proceedings of the 31st international conference on neural information processing systems (NIPS'17)* (pp. 4768–4777). Curran Associates Inc.

Lundberg, S. M., & Lee, S.-I. (2017b). A unified approach to interpreting model predictions. *Advances in Neural Information Processing Systems, 30*, 4765–4774. https://doi.org/10.48550/arXiv.1705.07874

Magarelli, M., Grassi, S., Squeo, G., Novielli, P., Bellotti, R., Caponio, F., Alamprese, C., & Tangaro, S. (2026). Unlocking extra virgin olive oil identification: Predicting ethyl esters with explainable AI on IR spectra. *Food Chemistry, 498*(Part 1), Article 147013. https://doi.org/10.1016/j.foodchem.2025.147013

Magarelli, M., Novielli, P., De Filippis, F., Magliulo, R., Di Bitonto, P., Diacono, D., … Tangaro, S. (2024). Explainable artificial intelligence and microbiome data for food geographical origin: The mozzarella di Bufala Campana PDO case study. *Frontiers in Microbiology, 15*, Article 1393243. https://doi.org/10.3389/fmicb.2024.1393243

Marini, F. (2009). Artificial neural networks in foodstuff analyses: Trends and perspectives. A review. *Analytica Chimica Acta, 635*(2), 121–131. https://doi.org/10.1016/j.aca.2009.01.009

Müller, M.-S., Oest, M., Scheffler, S., Horns, A. L., Paasch, N., Bachmann, R., & Fischer, M. (2024). Food authentication Goes green: Method optimization for origin discrimination of apples using apple juice and ICP-MS. *Foods, 13*(23), 3783. https://doi.org/10.3390/foods13233783

Nguyen, Q. T., Nguyen, T. T., Le, V. N., Nguyen, N. T., Truong, N. M., Hoang, M. T., … Bui, Q. M. (2023). Towards a standardized approach for the geographical traceability of plant foods using inductively coupled plasma mass spectrometry (ICP–MS) and principal component analysis (PCA). *Foods, 12*(9), Article 1848. https://doi.org/10.3390/foods12091848

Nikezić, M., Chantzi, P., Irrgeher, J., & Zuliani, T. (2024). Evaluating source complexity in blended milk cheese: Integrated strontium isotope and multi-elemental approach to PDO Graviera Naxos. *Foods, 13*(16), 2540. https://doi.org/10.3390/foods13162540

Nikezić, M., Perşoiu, A., Feher, R., Popa, I., & Zuliani, T. (2024). Geochemical fingerprinting of Norway spruce from the eastern Carpathians: Sr isotopic and multi-elemental signatures. *Science of the Total Environment, 954*, Article 176244. https://doi.org/10.1016/j.scitotenv.2024.176244

Ning, Y., Ong, M. E. H., Chakraborty, B., Goldstein, B. A., Ting, D. S. W., Vaughan, R., & Liu, N. (2022). Shapley variable importance cloud for interpretable machine learning. *Patterns, 3*(4), Article 100452. https://doi.org/10.1016/j.patter.2022.100452

Patacca, E., & Scandone, P. (2007). Geology of the southern Apennines. *Bollettino della Società Geologica Italiana (Italian journal of geosciences), Special Issue 7*, 75–119.

Pedregosa, F., Varoquaux, G., Gramfort, A., Michel, V., Thirion, B., Grisel, O., Blondel, M., Prettenhofer, P., Weiss, R., Dubourg, V., VanderPlas, J., Passos, A., Cournapeau, D., Brucher, M., Perrot, M., & Duchesnay, É. (2011). Scikit-learn: Machine learning in Python. *Journal of Machine Learning Research, 12*, 2825–2830. https://jmlr.org/papers/v12/pedregosa11a.html.

Chemistry of Europe's agricultural soils: Part a – Methodology and interpretation of the GEMAS data set. In Reimann, C., Birke, M., Demetriades, A., Filzmoser, P., & O'Connor, P. (Eds.), *Geologisches Jahrbuch Reihe B 102*, (2014). E. Schweizerbart Science Publishers.

Roberts, J. J., & Cozzolino, D. (2016). An overview on the application of chemometrics in food science and technology–an approach to quantitative data analysis. *Food Analytical Methods, 9*, 3258–3267. https://doi.org/10.1007/s12161-016-0574-7

Saar de Almeida, B., Fedele, L., D'Antonio, M., Morra, V., Mercurio, M., Stevenson, R., & Widory, D. (2023). Characterizing wine terroir using strontium isotope ratios: A review. *Isotopes in Environmental and Health Studies, 59*(4–6). https://doi.org/10.1080/10256016.2023.2245122

Schaffer, C. (1993). Selecting a classification method by cross-validation. *Machine Learning, 13*(2–3), 135–143. https://doi.org/10.1007/BF00993106

Schneider, M., Keiblinger, K. M., Paumann, M., Soja, G., Mentler, A., Golestani-Fard, A., … Zehetner, F. (2019). Fungicide application increased copper-bioavailability and impaired nitrogen fixation through reduced root nodule formation on alfalfa. *Ecotoxicology, 28*(6), 599–611. https://doi.org/10.1007/s10646-019-02047-9

Stantis, C., Willmes, M., Le Corre, M., James, H. F., Kafino, C., Verostick, K. A., … Bataille, C. P. (2026). Global compilation of bioavailable strontium isotope data. *Scientific Data, 13*, Article 299. https://doi.org/10.1038/s41597-026-06643-3

Telloli, C., Cicconi, F., Manzi, E., Borgognoni, F., Salvi, S., Iapalucci, M. C., & Rizzo, A. (2024). Multi-elemental analysis of commercial wheat flours by ICP–MS triple quadrupole in function of the milling degree. *Food Chemistry, 450*, Article 139370. https://doi.org/10.1016/j.foodchem.2024.139370

Thabit, T. M. A. M., Shokr, S. A., Elgeddawy, D. I. H., & El-Naggar, M. A. H. (2020). Determination of heavy metals in wheat and barley grains using ICP–MS/MS. *Journal of AOAC International, 103*(5), 1277–1281. https://doi.org/10.1093/jaoacint/qsaa029

Tommasini, S., Marchionni, S., Tescione, I., Casalini, M., Braschi, E., Avanzinelli, R., & Conticelli, S. (2018). Strontium isotopes in biological material: A key tool for the geographic traceability of foods and human beings. In D. K. Gupta, & C. Walther (Eds.), *Behaviour of strontium in plants and the environment* (pp. 145–166). Cham: Springer. https://doi.org/10.1007/978-3-319-66574-0_10.

Tsirogiannis, G., Zotos, A., Mazarakioti, E. C., Kokkotos, E., Kontogeorgos, A., Patakas, A., & Ladavos, A. (2023). A statistical approach to identify appropriate sampling scheme capable of geographical identification analysis of the protected origin pulse crops in Greece. *Applied Sciences, 13*(6), 3623. https://doi.org/10.3390/app13063623

Vai, G. B., & Martini, I. P. (2001). *Anatomy of an orogen: The Apennines and adjacent Mediterranean basins*. Kluwer Academic Publishers. https://doi.org/10.1007/978-94-015-9829-3

Voerkelius, S., Lorenz, G. D., Rummel, S., Quétel, C. R., Heiss, G., Baxter, M., … Ueckermann, H. (2010). Strontium isotopic signatures of natural mineral waters, the reference to a simple geological map and its potential for authentication of food. *Food Chemistry, 118*(4), 933–940. https://doi.org/10.1016/j.foodchem.2009.04.125

Wang, M., Jiang, Y., Han, X., Ren, A., He, J., Yin, M., … Peng, H. (2025-2026). Fine-scale strontium isotope mapping in eastern China (Anhui Province) and its application in food traceability. *Foods, 15*(1), 33. https://doi.org/10.3390/foods15010033

White, P. J., & Broadley, M. R. (2009). Biofortification of crops with seven mineral elements often lacking in human diets - Iron, zinc, copper, calcium, magnesium, selenium and iodine. *New Phytologist, 182*(1), 49–84. https://doi.org/10.1111/j.1469-8137.2008.02738.x

Won, E.-J., Kim, S. H., Go, Y.-S., Kumar, K., Kim, M.-S., Yoon, S.-H., … Shin, K. (2021). A multi-elements isotope approach to assess the geographic provenance of Manila clams (*Ruditapes philippinarum*) via recombining appropriate elements. *Foods, 10*(3), 646. https://doi.org/10.3390/foods10030646

Yang, Y., Zhang, M., Ma, H., Lin, C., Wang, Z., Ma, B., & Wang, L. (2026). Novel pectic-dominated cell wall polysaccharides from fresh Rehmannia radix: Physicochemical and rheological characteristics, antioxidant-immunomodulation dual activities, and structure-activity relationship analysis. *Food Bioscience, 80*, Article 108893. https://doi.org/10.1016/j.fbio.2026.108893

Zhao, F. J., Su, Y. H., Dunham, S. J., Rakszegi, M., Bedő, Z., McGrath, S. P., & Shewry, P. R. (2009). Variation in mineral micronutrient concentrations in grain of wheat lines of diverse origin. *Journal of Cereal Science, 49*(2), 290–295. https://doi.org/10.1016/j.jcs.2008.11.007

Zhao, H., Guo, B., Wei, Y., & Zhang, B. (2013). Multi-element composition of wheat grain and provenance soil and their potentialities as fingerprints of geographical origin. *Journal of Cereal Science, 57*(3), 391–397. https://doi.org/10.1016/j.jcs.2013.01.008

Zhao, H., Guo, B., Wei, Y., Zhang, B., Sun, S., Zhang, L., & Yan, J. (2011). Determining the geographic origin of wheat using multielement analysis and multivariate statistics. *Journal of Agricultural and Food Chemistry, 59*(9), 4397–4402. https://doi.org/10.1021/jf200108d